

M. Tavakoli

Department of Electrical and Computer Engineering,
University of Alberta,
Edmonton, AB,
Canada
tavakoli@ece.ualberta.ca

Robert D. Howe

BioRobotics Laboratory,
School of Engineering and Applied Sciences,
Harvard University,
Cambridge, MA,
USA
howe@seas.harvard.edu

Haptic Effects of Surgical Teleoperator Flexibility

Abstract

Minimally invasive surgery systems typically involve thin and cable-driven surgical instruments. This introduces link and joint flexibility in the slave robot of a master–slave teleoperation system, reducing the effective stiffness of the slave and the transparency of teleoperation. In this paper, we analyze transparency under slave link and joint flexibility (tool flexibility). We also evaluate the added benefits of using extra sensors at the tip of the flexible robot. It is shown that tip velocity (or position) feedback improves free-space position tracking performance in the presence of robot flexibility. Also, when the interaction forces with an environment are measured by a force sensor and fed back to the user's hand, tip velocity feedback improves hard-contact force tracking performance. During a hard contact task, tip velocity feedback can also eliminate the transmission of robot flexibility to the user's hand.

KEY WORDS—haptic surgery teleoperation, link flexibility, joint flexibility, transparency, stability

1. Introduction

In applications such as space and surgical robotics, it is advantageous to use thin and lightweight manipulators and

cable-driven end-effectors. Space robots are designed to be lightweight and compact for minimum liftoff cost and energy consumption during robot control, and therefore involve flexibility. Surgical robots have thin instruments that enter the patient's body through ports for minimal invasiveness, which brings about advantages such as reduced trauma to the body, post-operative pain and length of hospital stay. An example is the Zeus Surgical Robot System (Figure 1) from Computer Motion Inc., Goleta, CA, USA, in which a 1 N force applied to the tip of one of its cantilevered instruments (straight endoscissors) causes a 15 mm tip deflection (Beasley and Howe, 2005). As the surgical instruments become thinner (e.g. less than 3 mm in pediatric surgery), the effect of flexibility becomes more crippling. Moreover, owing to space limitations and the small diameter of the instruments in minimally invasive surgery, actuation of a distal wrist that is used for dexterity is performed from outside the patient and propagated to the wrist through flexible cables. Therefore, in addition to link flexibility, joint flexibility is often present in surgical robots. In addition to flexibility, there are other non-idealities that exist in practice and need to be accounted for including communication latency (Niemeyer and Slotine, 2004; Aziminejad et al., 2007; Pressman et al., 2007; Ohnishi and Mochizuki, 2007), encoder quantization (Abbott and Okamura, 2005), discrete-time implementation of haptic control laws (Gil et al., 2004; Love and Book, 1995; Tavakoli et al., 2007b), friction (Abbott and Okamura, 2005; Diolaiti et al., 2006), backlash, and noise.

In the presence of link or joint flexibility, control laws based on the assumption of a rigid robot may no longer be effective.

The International Journal of Robotics Research
Vol. 00, No. 00, Xxxxxxxx 2009, pp. 000–000
DOI: 10.1177/0278364909101231
© The Author(s), 2009. Reprints and permissions:
<http://www.sagepub.co.uk/journalsPermissions.nav>
Figures 1–5, 7–9 appear in color online: <http://ijr.sagepub.com>

Parts of this research have previously been published as Tavakoli and Howe (2007) and Tavakoli and Howe (2008).



Fig. 1. The Zeus Surgical Robot System.

tive or accurate due to the alteration of the kinematic and dynamic characteristics of the manipulator. Without compensation, flexibility may cause steady-state errors, transient errors and vibrations, and even instability in the system. Dwivedy and Eberhard (2006) provided an extensive survey of the literature related to the dynamic analysis and control of flexible-joint and flexible-link robots. An example application in which joint flexibility needs to be compensated for is capturing non-cooperative objects such as space debris, where high-bandwidth control is required (Nishida and Yoshikawa, 2003). The pioneering work by Cannon and Schmitz (1984) pertained to the control of flexible-link robots when the sensors and actuators are not co-located. Beasley and Howe (2005) proposed a model-based method to reduce the kinematic errors in the control of a flexible surgical instrument.

Diaz and Gil (2008) analyzed the stability boundary of haptic rendering when the haptic user interface has internal vibration modes due to cable transmissions. For the specific problem of teleoperation with a low-stiffness slave, Christiansson and van der Helm (2007) performed experiments with a 1-DOF master–slave system to demonstrate teleoperation performance/stability trade-offs. As metrics of performance, they measured the low-frequency asymptotes ($\lim_{s \rightarrow 0}$) of the impedance transmitted to the operator when the slave is in free space and the impedance transmitted to the operator when the slave is in contact with a stiff environment. For quantifying a margin of stability, increasing amounts of delay were injected between the master and the slave until the teleoperation system approached the verge of instability. They concluded that the two performance metrics deteriorate in the presence of flexibility but this performance loss can be partly compensated

for by incorporating deflection information in the control laws, and that the stability margin increases if the slave stiffness decreases.

In this paper, we systematically analyze performance and stability limitations under link or joint flexibility (tool flexibility) in the slave robot of a master–slave teleoperation system, and examine what added benefits tip sensors can deliver. This general analytical treatment considers the following four measures of performance: free-motion transmitted impedance, free-motion position tracking, hard-contact force tracking metric, and hard-contact transmitted impedance. Two teleoperation architectures, position-error-based (PEB) control and direct force reflection (DFR) control, are considered mainly because of their implementation simplicity and widespread use. For both teleoperation control methods, we examine the effect of position and/or force sensors at the tip of a flexible slave on the above four performance metrics across the whole frequency range (i.e. for all s) and investigate the effect on the bandwidths of position and force tracking responses. We also conduct an analysis of absolute stability (stability under all passive but otherwise arbitrary human operators and remote environments) for the possible combinations of teleoperation methods and sensor configurations.

2. Criteria for Analysis of Teleoperation Transparency and Stability

For consistency with the teleoperation literature and without loss of generality, we use velocities rather than positions in models and control laws¹. In an ideal 1-DOF master–slave teleoperation system with hand-master velocity v_h and slave-environment velocity v_e , as in Figure 2(a), the dynamics of the master and the slave are

$$f_m + f_h = M_m \dot{v}_h, \quad f_s - f_e = M_s \dot{v}_e, \quad (1)$$

where f_h and f_e denote the forces exerted by the operator's hand on the master and by the environment on the slave, respectively. Here M_m , M_s , f_m and f_s are the master and the slave inertias and control signals, respectively.

2.1. Performance Measures

In an *ideally transparent* teleoperation system (Hannaford, 1989), through appropriate control outputs f_m and f_s , the positions and contact forces at the master and the slave ends will match regardless of the operator and environment dynamics

$$v_h = v_e, \quad f_h = f_e. \quad (2)$$

1. Note, however, the possibility of a steady-state error between the master and slave positions when they have the same velocities. For an investigation of position drift in bilateral teleoperation, see Chopra et al. (2006); Ching and Book (2006)

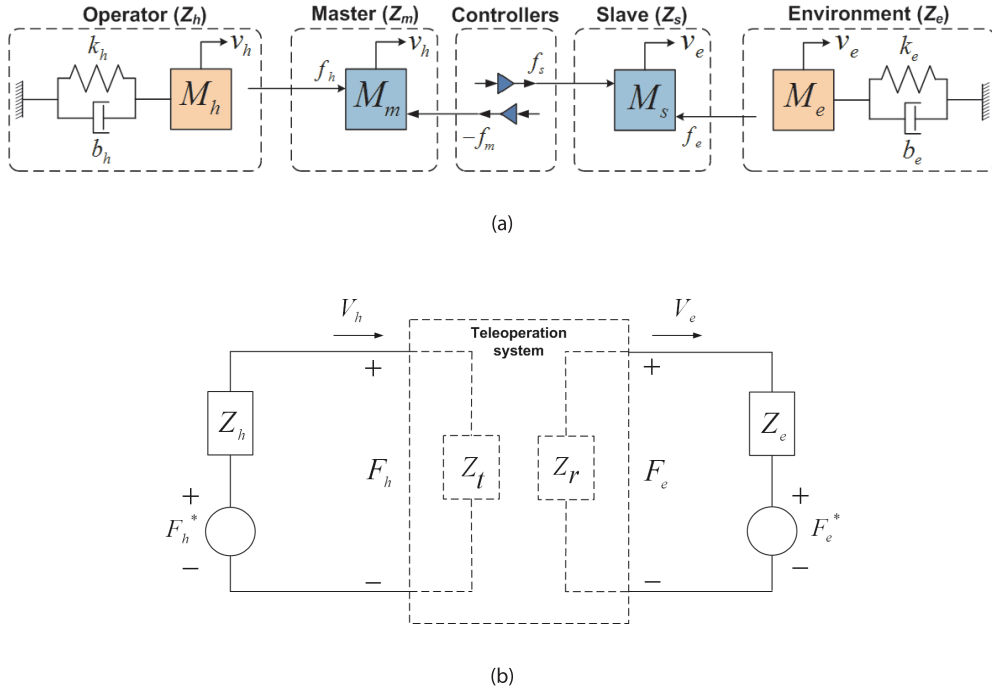


Fig. 2. (a) Physical and (b) two port s -domain representations of a teleoperation system.

Condition Equation (2) guarantees that the dynamics of the environment is displayed to the user with no distortion.

By considering Laplace transforms $V(s)$ and $F(s)$ of the velocities and forces in a teleoperation system, an equivalent representation of the system can be obtained (Hannaford, 1989) (Figure 2(b)), in which impedances $Z_h(s)$ and $Z_e(s)$ denote dynamic characteristics of the human operator's hand and the remote environment, respectively. Here, F_h^* and F_e^* are respectively the operator's and the environment's exogenous input forces and are independent of teleoperation system behavior. With the s -domain hybrid representation of a teleoperation system (Hannaford, 1989)

$$\begin{bmatrix} F_h(s) \\ -V_e(s) \end{bmatrix} = \begin{bmatrix} h_{11} & h_{12} \\ h_{21} & h_{22} \end{bmatrix} \begin{bmatrix} V_h(s) \\ F_e(s) \end{bmatrix}, \quad (3)$$

Equation (2) can be expressed as

$$H_{\text{ideal}} = \begin{bmatrix} 0 & 1 \\ -1 & 0 \end{bmatrix}. \quad (4)$$

Limiting cases of two elements of the H matrix,

$$h_{11} = \frac{F_h}{V_h}|_{F_e=0}, \quad h_{21} = -\frac{V_e}{V_h}|_{F_e=0}, \quad (5)$$

have direct physical significance. The parameter h_{11} is the impedance transmitted to the user (input impedance) when

$F_e = 0$, i.e. the slave is in free space ($\rightarrow 0$ ideally). Non-zero values for h_{11} mean that the teleoperation system is providing the user with non-zero forces during free-motion movements. The parameter h_{21} is a measure of velocity tracking fidelity when the slave is in free space ($\rightarrow -1$ ideally). Limiting cases of the other two parameters, i.e.

$$h_{12} = \frac{F_h}{F_e}|_{V_h=0}, \quad h_{22} = -\frac{V_e}{F_e}|_{V_h=0}, \quad (6)$$

are measures of force tracking fidelity and the output admittance assuming that the master is in contact with an infinitely stiff hand. Instead of h_{12} and h_{22} , it is more useful to consider elements of the transmission and the impedance matrices (Aliaga et al., 2004)

$$f_{12} = \frac{F_h}{F_e}|_{V_e=0}, \quad z_{11} = \frac{F_h}{V_h}|_{V_e=0}. \quad (7)$$

The above parameters assume that the slave is in hard contact. The parameter f_{12} shows force tracking fidelity under hard contact ($\rightarrow 1$ ideally) and the parameter z_{11} is the maximum impedance that can be transmitted to the user ($\rightarrow \infty$ ideally), thus quantifying the realism of a user's haptic experience about touching a rigid surface.

Colgate and Brown (1994) proposed using the Z -width, defined as $z_{11} - h_{11}$, as a measure of performance ($\rightarrow \infty$ ideally). An ideal haptic teleoperation system accurately reproduces both free motion and hard contact at the slave for the

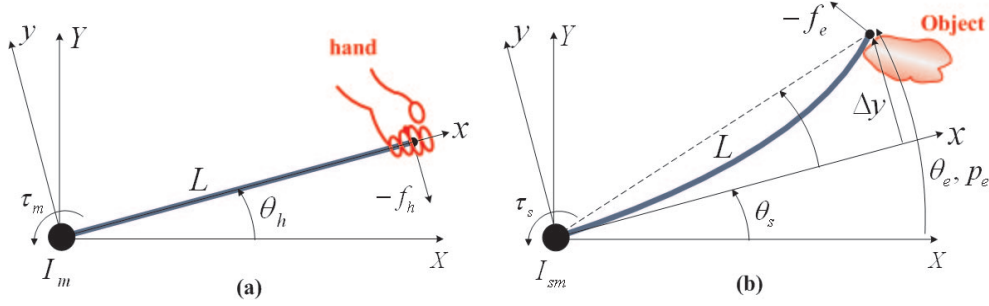


Fig. 3. (a) The master; (b) the flexible-link slave.

user. Another measure that is dependent on the hybrid parameters but provides important insight into the transparency of a teleoperation system is the environment impedance as transmitted to the user ($\rightarrow Z_e$ ideally)

$$Z_t = \frac{F_h}{V_h} = h_{11} - \frac{h_{12}h_{21}Z_e}{1 + h_{22}Z_e}. \quad (8)$$

2.2. Stability

For an analysis of the stability of a teleoperation system, knowledge of the human operator and the environment dynamics are needed in addition to the teleoperation system model (Equation (3)). However, assuming that $Z_h(s)$ and $Z_e(s)$ are passive, we may be able to find stability conditions independent of the human operator and the environment. The necessary and sufficient conditions for *absolute stability* (stability under all passive terminations $Z_h(s)$ and $Z_e(s)$) of a two-port network are given below.

Llewellyn's Criterion (Haykin, 1970)

The two-port system (Equation (3)) is absolutely stable if: (a) $h_{11}(s)$ and $h_{22}(s)$ have no poles in the right half plane (RHP); (b) any poles of $h_{11}(s)$ and $h_{22}(s)$ on the imaginary axis are simple with real and positive residues; and (c) for $s = j\omega$ and all real values of ω

$$\Re(h_{11}) \geq 0, \quad (9)$$

$$\Re(h_{22}) \geq 0, \quad (10)$$

$$2\Re(h_{11})\Re(h_{22}) - \Re(h_{12}h_{21}) - |h_{12}h_{21}| \geq 0, \quad (11)$$

where $\Re(\cdot)$ and $|\cdot|$ show the real part and the absolute value.

3. Teleoperator Model with Slave Flexibility

The forgoing analysis tools are applicable to general models of the slave robot. We now consider the case when the slave has a flexible coupling between the actuator and the end-effector.

3.1. The Case of a Flexible-link Slave

An ideal 1-DOF teleoperation system, in which the master is rigid but the slave has a flexible tool that couples the actuator to the end-effector, is shown in Figure 3, where I_m , I_{sm} , τ_m and τ_s are the master and the slave (excluding the flexible link) inertias and controller outputs, respectively. Also, $-f_h$ and $-f_e$ denote the forces exerted by the operator's hand on the master and by the environment on the slave, respectively. The hand-master position and the slave-environment position are denoted by θ_h and θ_e , respectively, while θ_s is used to show the slave's joint position, which is different from θ_e owing to the link flexibility. With a rigid link of length L and defining $\omega_h = \dot{\theta}_h$ and $\tau_h = Lf_h$, the dynamics of the master in Figure 3(a) are

$$I_m \dot{\omega}_h = \tau_m + \tau_h. \quad (12)$$

The exact dynamics of a flexible link are described by partial differential equations and have infinite dimensions. In the constrained assumed modes method, the deflection of the flexible link in Figure 3(b) is modeled as

$$\Delta y(x, t) = \sum_{i=1}^{\infty} F_i(x)q_i(t), \quad 0 \leq x \leq L, \quad (13)$$

where $q_i(t)$ are the assumed flexible modes and $F_i(x)$ are the corresponding time-independent modes shape functions. Considering the first mode $q_1(t)$, which is capable of capturing the dominant frequency (Zhu et al., 1999) presented a method for lumping the distributed mass of the flexible link to a point mass located at its tip followed by modeling the flexibility of the link by a massless linear bending spring. Denoting the equivalent tip lumped mass by M_{se} and the equivalent bending spring stiffness by K_s , the resulting lumped dynamic model of the flexible link in Figure 3(b) is

$$M_{se} \ddot{p}_e = -K_s \Delta y - f_e \quad (14)$$

and

$$I_{sm} \ddot{\theta}_s = \tau_s + LK_s \Delta y, \quad (15)$$

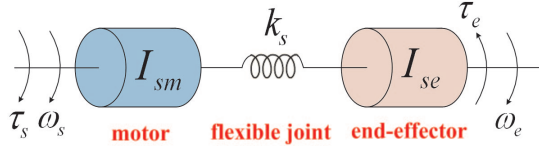


Fig. 4. Model of a flexible joint.

where $p_e = L\theta_s + \Delta y$ is the arc approximation of the link tip position assuming that Δy is small. Noting that $\theta_e = p_e/L$ and defining

$$\Delta\theta = \theta_s - \theta_e = -\Delta y/L, \quad (16)$$

$$I_{se} = M_{se}L^2, \quad (17)$$

$$k_s = K_sL^2, \quad (18)$$

$$\tau_e = Lf_e, \quad (19)$$

the lumped model in Equations (14)–(15) of the flexible-link slave in Figure 3(b) is rewritten as

$$I_{se}\dot{\omega}_e = k_s\Delta\theta - \tau_e, \quad (20)$$

$$I_{sm}\dot{\omega}_s = \tau_s - k_s\Delta\theta, \quad (21)$$

where $\omega_e = \dot{\theta}_e$ and $\omega_s = \dot{\theta}_s$.

Interestingly, the lumped dynamics (Equations (20)–(21)) of the flexible link are identical to the dynamics of the flexible joint shown in Figure 4 consisting of a motor with inertia I_{sm} and an end-effector with inertia I_{se} that are coupled via a shaft with a finite stiffness k_s . Therefore, a flexible-link slave affects teleoperation performance in the same way as an elastic-joint slave.

3.2. The Case of a Flexible-joint Slave

The compliance in the joint of a robot can be modeled by a chained mass–spring–damper system, in which the first mass represents the joint motor whose position is measured and the last mass represents the end-effector by which the robot makes contact with the environment (Spong, 1987; Mills, 1992). Figure 4 shows a rotational two-mass model with a spring. As it will be explained later, since we will be using a proportional-derivative (PD) position controller for the flexible robot, there is no need to include a damper in the model because such a damping term would contribute to the closed-loop equation in the same way as the derivative term of the PD controller. In this model, τ_s and ω_s are the slave's motor torque and speed, respectively. Also, ω_e is the slave's end-effector (and the environment's) speed and τ_e is the torque applied by the environment on the slave's end-effector.

In the context of teleoperation control under slave joint compliance, we are interested in control of the slave's end-effector position, which is different from the motor position at least in the transient state, thus position sensing at the end-effector is useful. Depending on the teleoperation architecture and for better performance, we may also need force sensing at the end-effector.

For compatibility with the common notations in the teleoperation literature, we use the equivalent *translational model* of the elastic joint in the rest of this paper including in Figure 5, which shows a master–slave system with an elastic-joint slave. The equations of motion of the elastic joint present in Figure 5 are

$$M_{sm}\dot{v}_s = f_s - k_s\Delta x, \quad (22)$$

$$M_{se}\dot{v}_e = -f_e + k_s\Delta x, \quad (23)$$

$$\Delta x = x_s - x_e, \quad (24)$$

where $v_s = \dot{x}_s$ and $v_e = \dot{x}_e$ are the slave's motor and end-effector velocities, respectively. Also, f_s is the force exerted by the slave's actuator on the elastic joint and f_e is exerted by the environment on the slave's end-effector. An s -domain model of this two-input/two-output system is depicted in Figure 6(c), in which $Z_{sm} = M_{sm}s$ and $Z_{se} = M_{se}s$.

Damping terms have not been considered in the master and the slave dynamics because such terms contribute to the closed-loop equations in the same way as the derivative terms of the master and slave PD controllers (C_m and C_s in Equation (29)), and therefore do not need to be considered separately. Also, to avoid complexities resulting from non-linear terms, we have not considered backlash or friction in this analysis. The master and slave robot actuators are assumed to have unlimited bandwidths compared to the maximum frequency of the desired operating trajectories.

A state-space model of the two-mass system is

$$\frac{d}{dt} \begin{pmatrix} v_s \\ \Delta x \\ v_e \end{pmatrix} = \begin{pmatrix} 0 & -\frac{k_s}{M_{sm}} & 0 \\ 1 & 0 & -1 \\ 0 & \frac{k_s}{M_{se}} & 0 \end{pmatrix} \begin{pmatrix} v_s \\ \Delta x \\ v_e \end{pmatrix} + \begin{pmatrix} \frac{1}{M_{sm}} \\ 0 \\ 0 \end{pmatrix} f_s + \begin{pmatrix} 0 \\ 0 \\ \frac{-1}{M_{se}} \end{pmatrix} f_e. \quad (25)$$

The above system is state-controllable, meaning that if all states (v_s , Δx and v_e) are measurable, the eigenvalues of the system can be relocated to stable positions via state feedback.

The system (Equation (25)) has one eigenvalue at the origin of the s -plane and two eigenvalues at $\pm j\omega_R$ where

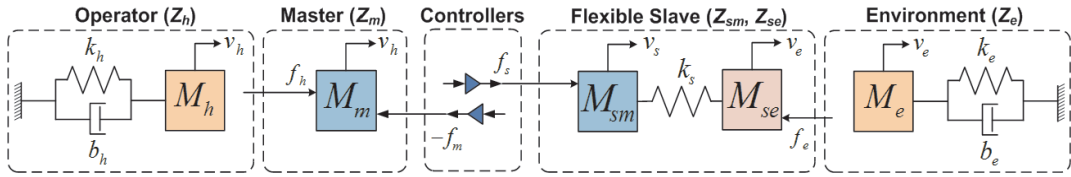


Fig. 5. Models of the operator, master, flexible slave, and environment.

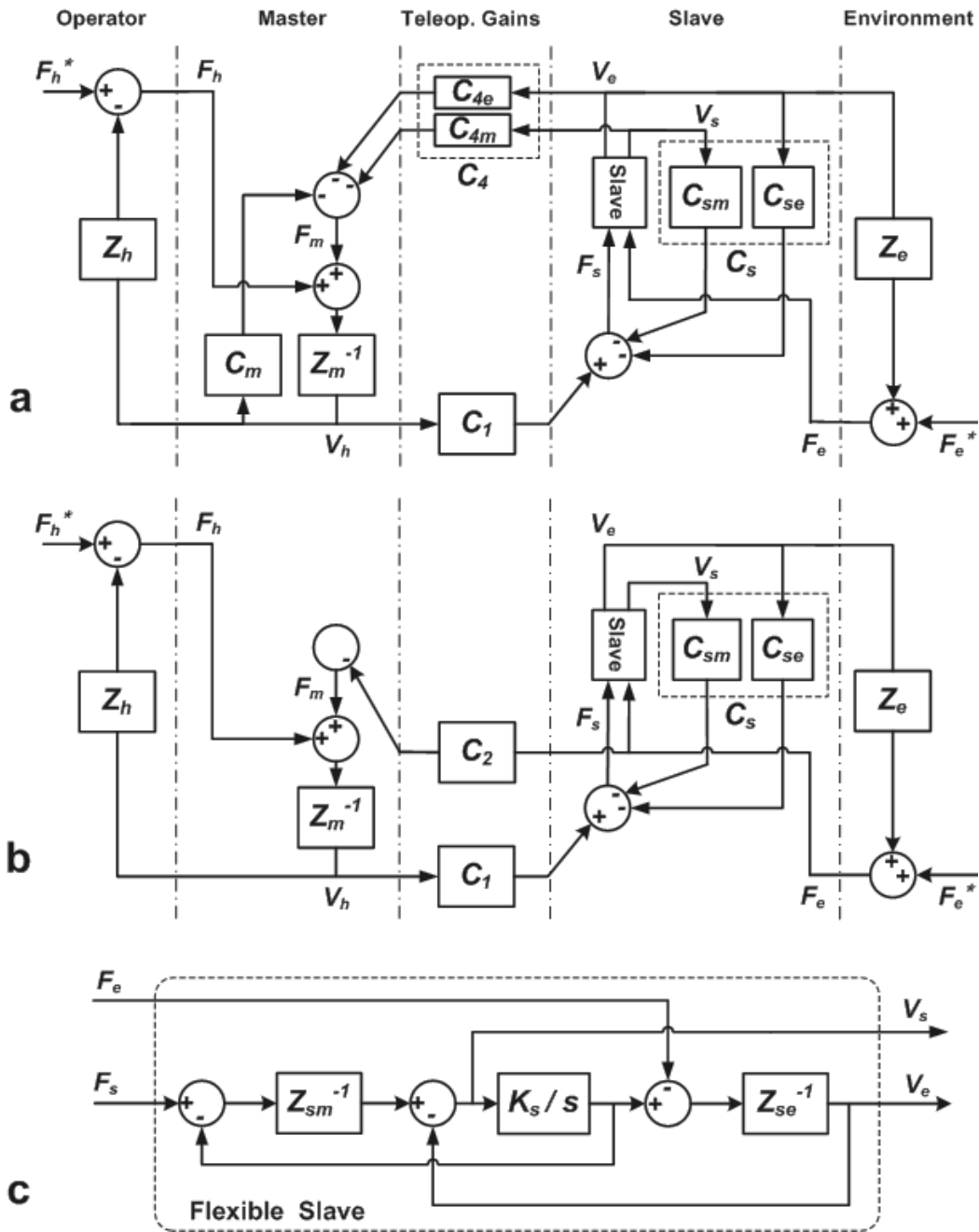


Fig. 6. (a) PEB architecture, (b) DFR architecture, and (c) dynamic model of a flexible slave.

$$\omega_R = \sqrt{k_s \left(\frac{1}{M_{sm}} + \frac{1}{M_{se}} \right)} \quad (26)$$

is the system resonance frequency. For the control input f_s , if v_s is the output, the system will have two zeros at $\pm j\omega_0$ where

$$\omega_0 = \sqrt{\frac{k_s}{M_{se}}} \quad (27)$$

is the system anti-resonance frequency. If v_e is taken as the output, however, the system will show no anti-resonant behavior.

In the context of vibration control of steel rolling mills, which also suffer from flexibility due to the long shafts and gear boxes and have a model similar to Equation (25), it has been shown that the inertia ratio,

$$R = \frac{M_{se}}{M_{sm}}, \quad (28)$$

plays a key role in shaping the dynamic characteristics of the elastic-joint system. When $R \ll 1$ and there is only feedback of v_s , the system has been reported to show a severely underdamped behavior (Zhang and Furusho, 2000). In this situation, although the oscillations in v_s may be small, those in v_e may be large. However, with feedback of end-effector velocity v_e , it is possible to dampen such oscillations. In the following section, we examine the effect of joint flexibility in a robot that is acting as the slave during haptic teleoperation.

4. Teleoperation Architectures versus Sensor Configurations

We now consider the relationship between the choice of the teleoperation control architecture (Tavakoli et al., 2007a) and the placement of sensors in a flexible slave. For a teleoperation architecture, different sensor configurations are possible. A velocity sensor on the slave's base (i.e. v_s feedback), a velocity sensor at the end-effector (i.e. v_e feedback), a force sensor at the end-effector (i.e. f_e feedback), or a combination of them makes up the different possibilities.

Consider the block diagrams in Figure 6, which represent two common teleoperation control architectures and in which $C_i(s)$ are controller transfer functions. PEB bilateral control shown in Figure 6(a) uses no force sensor measurements and merely tries to minimize the difference between the master and the slave positions for providing haptic feedback to the user. DFR bilateral control shown in Figures 6(b), however, employs a force sensor to measure slave-environment interactions for reflecting them to the user.

We assume that the environment is passive ($f_e^* = 0$ in Figures 6(a) and (b)) and the operator is passive in the sense that

he/she does not perform actions that will make the teleoperation system unstable. In Figures 6(a) and (b), the human operator's hand and the remote environment impedances are denoted by $Z_h(s)$ and $Z_e(s)$, respectively. Also, C_1 , C_4 , and

$$C_m = k_{pm} + k_{im}/s, \quad C_s = k_{ps} + k_{is}/s \quad (29)$$

are controllers (PI-type on velocities and PD-type on positions). The gain C_2 scales the slave/environment interaction as it is fed back to the master. In Figures 6(a) and (b), based on Equation (1), the master is represented as the impedance $Z_m^{-1} = 1/(M_m s)$. If the slave is rigid as in Equation (1), it is modeled by the impedance $Z_s^{-1} = 1/(M_s s)$. If the slave is flexible, the two-output model based on Equations (22)–(24) and shown in Figure 6(c) is used.

4.1. The Case of a Rigid Slave

Assuming a rigid slave, in the PEB control of Figure 6(a) we have $C_1 = C_s$ and $C_4 = -C_m$. Transparency can be improved by including "acceleration feedforward" terms, i.e. by choosing $C_1 = Z_s + C_s \doteq Z_{cs}$ and $C_4 = -Z_m - C_m \doteq -Z_{cm}$:

$$H = \begin{bmatrix} Z_m + C_m \frac{Z_s}{Z_{cs}} & \frac{C_m}{Z_{cs}} \\ -\frac{C_s}{Z_{cs}} & \frac{1}{Z_{cs}} \end{bmatrix},$$

$$H_{acc} = \begin{bmatrix} 0 & \frac{Z_{cm}}{Z_{cs}} \\ -1 & \frac{1}{Z_{cs}} \end{bmatrix}. \quad (30)$$

For simplicity, in this paper $C_m = C_s$ is chosen.

Similarly, for a rigid slave, in the DFR control of Figure 6(b), we have $C_1 = C_s$ and $C_2 = 1$. Again, transparency is improved by including acceleration feedforward ($C_1 = Z_{cs}$):

$$H = \begin{bmatrix} Z_m & 1 \\ -\frac{C_s}{Z_{cs}} & \frac{1}{Z_{cs}} \end{bmatrix}, \quad H_{acc} = \begin{bmatrix} Z_m & 1 \\ -1 & \frac{1}{Z_{cs}} \end{bmatrix}. \quad (31)$$

4.2. The Case of a Flexible Slave

In this case, since the flexible slave model has two outputs as shown in Figure 6(c), C_s and C_4 in Figures 6(a) and (b) are each broken into two separate controllers. Depending on the placement of sensors as discussed before, C_s and C_4 should be replaced by either C_{sm} or C_{se} and either C_{4m} or C_{4e} .

The general control laws for the master in PEB and DFR architectures are defined as

$$F_m = -C_m V_h - (C_{4m} V_s + C_{4e} V_e) \quad (\text{see Figure 6(a)}), \quad (32)$$

$$F_m = -C_2 F_e \quad (\text{see Figure 6(b)}), \quad (33)$$

respectively. The control law for the slave in both PEB and DFR is defined as

$$F_s = C_1 V_h^* - (C_{sm} V_s + C_{se} V_e) \quad (34)$$

(see Figure 6(a) and (b)).

The desired slave velocity v_h^* in Equation (34) is normally equal to the operator's hand velocity v_h . However, with feedback of v_s and f_e , it is possible to calculate v_h^* more accurately based on the open-loop system Equation (23). Taking the time derivative of both sides of Equation (23) gives $M_{se}\ddot{v}_e = k_s(v_s - v_e) - \dot{f}_e$. Since $v_e = v_h$ is the performance goal, the estimated desired trajectory for v_s becomes

$$v_h^* = v_h + (M_{se}/k_s)\ddot{v}_h + \dot{f}_e/k_s. \quad (35)$$

This estimate relies on derivatives of acceleration and force, which may be problematic to implement. We therefore consider teleoperator performance both with and without this estimate in Section 5 below. In the following section, we examine the effect of flexibility in a slave robot during haptic teleoperation.

5. Performance Measures

5.1. PEB Control Based on Feedback of v_s

With no feedback of v_e , we have $C_{se} = C_{4e} = 0$ in Figure 6(a). The PEB control with feedback of v_s is designed as follows. We choose identical local PI controllers $C_m = C_{sm} = k_p + k_i/s$, and $C_{4m} = -Z_m - C_m$. Since the flexible slave is comprised of two inertias, we consider the general form

$$C_1 = \eta_1 Z_{sm} + \eta_2 Z_{se} + C_{sm}, \quad (36)$$

where η_1 and η_2 are non-negative constants. As a result, the parameter h_{21} involves terms such as $k_i + k_p s + \eta_1 M_{sm} s^2 + \eta_2 M_{se} s^2$ in both its numerator and denominator, motivating the selections $\eta_1 = 1$, $\eta_2 = 0$, $k_i = \beta^2 M_{sm}$ and $k_p = 2\beta M_{sm}$ (which ensure critical damping) where $\beta > 0$ is a control gain determining the placement of poles in the system.

The resulting four measures of transparency defined in Section 2.1 are

$$h_{11} = M_{se} s \frac{1 + (R' - 1)(s/(s + \beta))^2}{1 + (s/\omega_0)^2 + R s^2 (s/(s + \beta))^2}, \quad (37)$$

$$h_{21} = \frac{-1}{1 + (s/\omega_0)^2 + R(s/(s + \beta))^2}, \quad (38)$$

$$\frac{1}{f_{12}} = \frac{1}{1 + (R' - 1)(s/(s + \beta))^2}, \quad (39)$$

$$z_{11} = M_{se} s \frac{1 + (R' - 1)(s/(s + \beta))^2}{(s/\omega_0)^2 + R(s/(s + \beta))^2}, \quad (40)$$

where

$$R' = \frac{M_m}{M_{sm}} \quad (41)$$

and ω_0 and R have been defined in Equations (27) and (28), respectively. The reason for using $1/f_{12}$ is to have a proper transfer function because in the presence of flexibility the order of the numerator of f_{12} increases. It can be seen that if $k_s \rightarrow \infty$ and $R \rightarrow 0$, the parameters corresponding to the rigid case (e.g. h_{11} and h_{21} of H_{acc} in Equation (30)) will be retrieved.

Assuming the PI controller $C_m = C_{sm}$ does not become saturated, the control parameter β can be selected to be sufficiently large so that the dynamics contributed by the controller (i.e. involving $(s + \beta)^2$) is much faster than the one originating from the rest of the system including joint flexibility. With this assumption, we get the simplified performance indices listed in the second column of Table 1.

While the above four parameters only depend on the teleoperation system, the impedance transmitted to the user is also a function of the environment impedance Z_e . Assuming a linear spring model $Z_e = k_e/s$ for the environment (i.e. $M_e = 0$ and $b_e = 0$ in Figure 5),

$$Z_t = \frac{1/s}{1/k_s + (1/k_e)/(1 + M_{se}/k_e s^2)}. \quad (42)$$

The transmitted impedance represents the combined effect of h_{11} and z_{11} . Evidently, when the slave is in free space ($k_e \rightarrow 0$), we will have $Z_t \rightarrow h_{11}$, and when it is in contact with a hard environment ($k_e \rightarrow \infty$), then $Z_t \rightarrow z_{11}$.

5.2. PEB Control Based on Feedback of v_e

With feedback of v_e , we have $C_{sm} = C_{4m} = 0$ in Figure 6(a). Again, $C_m = C_{se} = k_p + k_i/s$, $C_{4e} = -Z_m - C_m$, and $C_1 = \eta_1 Z_{sm} + \eta_2 Z_{se} + C_{se}$. For reasons similar to the case with feedback of v_s , we choose $\eta_1 = 1$, $\eta_2 = 0$, $k_i = \beta^2 M_{sm}$ and $k_p = 2\beta M_{sm}$. The transparency indices for PEB control with feedback of v_e when β is sufficiently large are listed in the third column of Table 1.

5.3. DFR Control Based on Feedback of v_s and f_e

With feedback of v_s , we have $C_{se} = 0$ in Figure 6(b). Also, $C_{sm} = k_p + k_i/s$, C_1 is chosen as in PEB control, and $C_2 = 1$. Depending on whether the desired v_s is taken to be v_h or calculated from Equation (35), the simplified transparency indices for large β are listed in the fourth and the fifth columns of Table 1, respectively.

5.4. DFR Control Based on Feedback of v_e and f_e

With feedback of v_e , we have $C_{sm} = 0$ in Figure 6(b). Also, $C_2 = 1$ and $C_{se} = k_p + k_i/s$. With C_1 chosen as in PEB control, the corresponding transparency indices for large β are listed in Table 1.

Table 1. Performance indices of different teleoperation architectures and sensor configurations when $\beta \rightarrow \infty$.

Teleoperation architecture	PEB	PEB	DFR	DFR	DFR	DFR	Ideal
Sensor measurements	v_s	v_e	v_s, f_e	v_s, f_e with Equation (35)	v_e, f_e	v_s, v_e, f_e with Equation (35)	
h_{11} (free-motion transmitted impedance)	$\frac{M_{se}s}{1+(\frac{s}{\omega_0})^2}$	$M_{se}s + M_{sm}^2s(\frac{s}{\omega_0})^2$	M_ms	M_ms	M_ms	M_ms	0
h_{21} (free-motion position tracking)	$\frac{-1}{1+(\frac{s}{\omega_0})^2}$	-1	$\frac{-1}{1+(\frac{s}{\omega_0})^2}$	-1	-1	-1	-1
$\frac{1}{f_{12}}$ (hard-contact force tracking)	1	$\frac{1}{1+\frac{1}{R}(\frac{s}{\omega_0})^2}$	$\frac{1}{1+\frac{Rl}{R}(\frac{s}{\omega_0})^2}$	1	1	1	1
z_{11} (hard-contact transmitted impedance)	$\frac{k_s}{s}$	∞	$M_ms + \frac{k_s}{s}$	∞	∞	∞	∞
Absolutely stable	Yes	No	Yes for $\omega < \omega_0$	Yes	No	Yes	

5.5. DFR Control with Feedback of v_s , v_e and f_e :

Since we have both v_s and v_e and we can also determine distinct desired trajectories for each of them due to the availability of f_e information, we employ a two-loop PI controller as proposed in Zhu et al. (1999) for the slave:

$$F_s = (C_{1m}V_h^* - C_{sm}V_s) + (C_{1e}V_h - C_{se}V_e). \quad (43)$$

Here, V_h^* is obtained from Equation (35), $C_{1m} = Z_{sm} + C_{sm}$ and $C_{1e} = Z_{se} + C_{se}$.

6. Effect of Flexibility on Transparency and Stability

The transparency indices listed in Table 1 are idealized to ignore the effect of controller dynamics by assuming $\beta \rightarrow \infty$, which corresponds to perfect local position control of the slave (and the master during PEB control). This is a simplification that is made to isolate the effect of robot flexibility. With this assumption, Section 6.1 is aimed at understanding the fundamental limitations imposed by robot flexibility on teleoperation transparency and the added benefits of using extra sensors at the output shaft of an elastic-joint robot or at the tip of a flexible-link robot. In practice, however, β cannot be infinitely large, thus bringing in the controller dynamics and limiting the performance. In Section 6.2, we investigate the effect of limited control action on transparency, specifically the indices for motion tracking and force tracking.

6.1. Transparency Assuming no Actuator Saturation

Based on Table 1, which assumes β is very large, the following conclusions can be drawn:

- For free-motion transmitted impedance (h_{11} , third row), during PEB teleoperation the user will feel some residual impedance that depends on the slave's mass and stiffness characteristics, while during DFR teleoperation only the master inertia will be transmitted to the user. If acceleration feedforward were not provided during PEB, the user would feel the master inertia as well.
- For free-motion position tracking (h_{21} , fourth row), with feedback of v_e , perfect position tracking can be attained in both PEB and DFR teleoperation regardless of the robot flexibility. With feedback of v_s , perfect position tracking in DFR teleoperation is possible if the desired trajectory for v_s is determined from Equation (35). Otherwise, position tracking with ω_s feedback is satisfactory only at low frequencies ($\omega < \omega_0$).
- For hard-contact force tracking ($1/f_{12}$, fifth row), perfect force tracking can be attained in PEB teleoperation with feedback of v_s . In DFR teleoperation, perfect force tracking is possible with feedback of v_e and/or feedback of v_s provided that Equation (35) is used for generating the desired trajectory of v_s . Otherwise, force tracking is satisfactory only in low frequencies.
- For hard-contact transmitted impedance (z_{11} , sixth row), with knowledge of v_s only, the flexibility in the slave will be felt by the user during a hard contact task unless Equation (35) is used for generating the desired trajectory of v_s . With feedback of v_e , however, hard surfaces can be displayed transparently to the user in both PEB and DFR teleoperation.

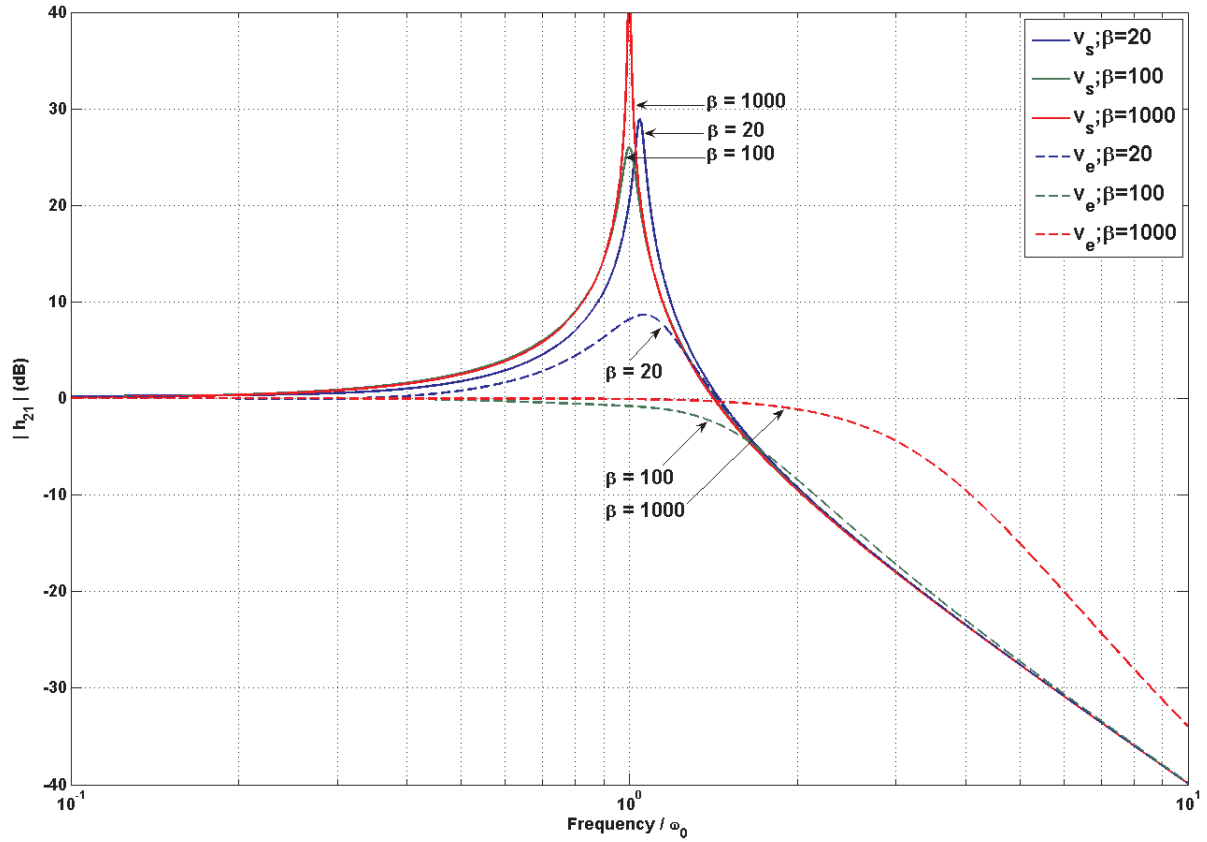


Fig. 7. Magnitude of h_{21} with feedback of v_s (solid lines) and feedback of v_e (dashed lines) versus normalized frequency when $R = 0.1$.

6.2. Effect of Avoiding Actuator Saturation on Transparency

Table 1 is accurate only for $\beta \rightarrow \infty$, but these relative performance characterizations for different teleoperation architectures and sensor configurations also apply for the case that β is limited. Here we focus on the effect of β on motion tracking and force tracking. It was shown that with feedback of v_e and $\beta \rightarrow \infty$, it is possible to achieve ideal free-motion position tracking ($h_{21} = -1$) regardless of the robot flexibility. This is not possible with feedback of v_s even when $\beta \rightarrow \infty$ unless Equation (35) is used. Also, ideal hard-contact force tracking ($1/f_{12} = 1$) is possible with feedback of v_e in DFR teleoperation, which is not attainable with feedback of v_s even when $\beta \rightarrow \infty$ unless Equation (35) is used. In the following we examine the effect of β on h_{21} and $1/f_{12}$ for these two possible sensor configurations.

6.2.1. Free-motion Position Tracking

For teleoperation with feedback of v_s , h_{21} (for both PEB and DFR) is given by

$$h_{21}|_{v_s} = \frac{-1}{1 + (s/\omega_0)^2 + R(s/(s + \beta))^2}. \quad (44)$$

For teleoperation with feedback of v_e , the parameter h_{21} (for both PEB and DFR) is given as

$$h_{21}|_{v_e} = \frac{-1}{1 + (R + (s/\omega_0)^2)(s/(s + \beta))^2}. \quad (45)$$

The magnitudes of the above two responses are plotted in Figure 7 when $\omega_0 = 100 \text{ rad s}^{-1}$, $R = 0.1$ and $\beta = 20, 100, 1,000$. For v_s feedback, $h_{21}|_{v_s} \approx 1$ only for frequencies lower than ω_0 regardless of β . However, for v_e feedback, we can increase the maximum frequency below which $h_{21}|_{v_e} \approx 1$ by increasing β . Therefore, the frequency range of position tracking is improved if feedback of v_e is provided and high-gain controllers are used. This is consistent with the discussion in Section 3 that the two-mass system (Equation (25)) has an anti-resonance at ω_0 if v_s is the output but has no anti-resonance if v_e is the output. Therefore, the presence of a velocity (or position) sensor at the output shaft of the elastic joint facilitates high-bandwidth position tracking during both PEB and DFR teleoperation.

To further investigate the effect of β and R on the shape of h_{21} , in Figure 8 the cutoff frequency ω_c (the frequency at which the magnitude drops by -3 dB compared with low fre-

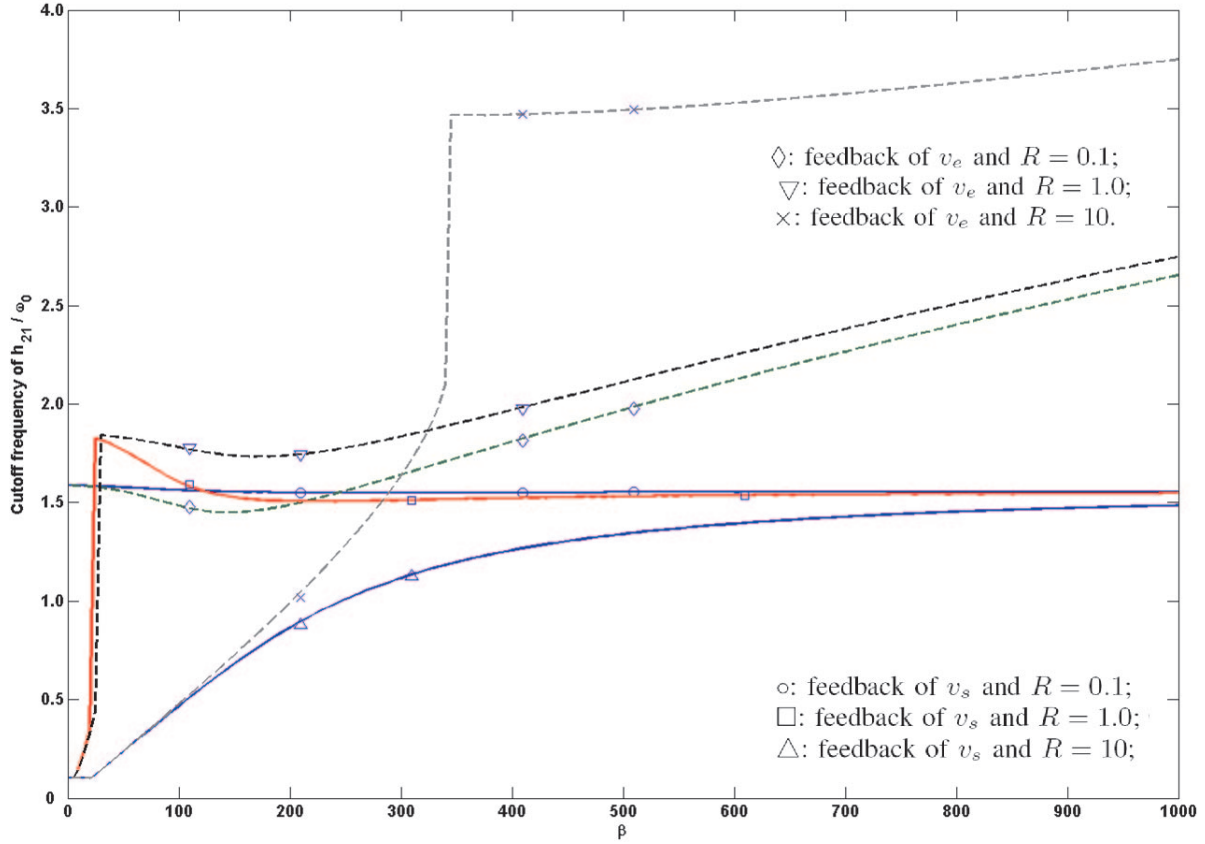


Fig. 8. Cutoff frequency of h_{21} with feedback of v_s (solid lines) and feedback of v_e (dashed lines) when $\omega_0 = 100 \text{ rad s}^{-1}$.

quencies) of h_{21} is plotted versus β for $\omega_0 = 100 \text{ rad s}^{-1}$, $R = 0.1, 1, 10$ and for feedback of v_s (solid lines) and feedback of v_e (dashed lines). As can be seen, with feedback of v_s , as $\beta \rightarrow \infty$ the cutoff frequency of h_{21} given by Equation (44) approaches $(\sqrt{2} + 1)^{1/2} \omega_0 = 1.55 \omega_0 \text{ rad s}^{-1}$. In contrast, with feedback of v_e , the cutoff frequency of h_{21} given by Equation (45) continues to grow as β increases, thus ensuring good position tracking over a wider frequency range. The other conclusion from Figure 8 is that when R is not small and β is not large (i.e. M_{se} is comparable to or larger than M_{sm} and the control effort applied on M_{sm} is limited), the position tracking bandwidth is severely limited even with feedback of v_e as the cutoff frequency of h_{21} drops below ω_0 . Therefore, as R gets larger, the need for higher control action (higher β) increases to attain satisfactory position tracking.

6.2.2. Hard-contact Force Tracking

In DFR teleoperation, $1/f_{12}$ for the two different position feedback possibilities is given by

$$\frac{1}{f_{12}} |_{\text{DFR}, v_s} = \frac{1}{1 + (R'/R)(s/\omega_0)^2 + R'(s/(s+\beta))^2}, \quad (46)$$

$$\frac{1}{f_{12}} |_{\text{DFR}, v_e} = \frac{1}{1 + (R'/R)(s/\omega_0)^2 + R'(s/(s+\beta))^2 + R'(s/(s+\beta))^2}, \quad (47)$$

Somewhat similar to the case with h_{21} , when we have feedback of v_s , near-ideal force tracking under hard-contact is obtained only for frequencies lower than $\omega_0 \sqrt{R/R'}$ regardless of the maximum control effort. In contrast, with v_e , the cutoff frequency of $1/f_{12}$ can be increased by increasing β . Therefore, in DFR teleoperation, feedback of v_e also helps to achieve high-bandwidth force tracking. The magnitudes of $1/f_{12}$ and the relationship between the cutoff frequency of $1/f_{12}$ and β are similar to those in Figures 7 and 8 for h_{21} , and are not shown here.

6.3. Absolute Stability Assuming no Actuator Saturation

From the last row of Table 1, obtained through examining Llewellyn's criterion for absolute stability, teleoperation with feedback of v_e alone is not absolutely stable. This is consistent with Vukosavic and Stojic (1998) that stability in servo drives similar to Figure 4 gets more difficult with load velocity feedback (v_e) as the closed-loop system will encompass torsional resonance modes. Nonetheless, in practice, friction

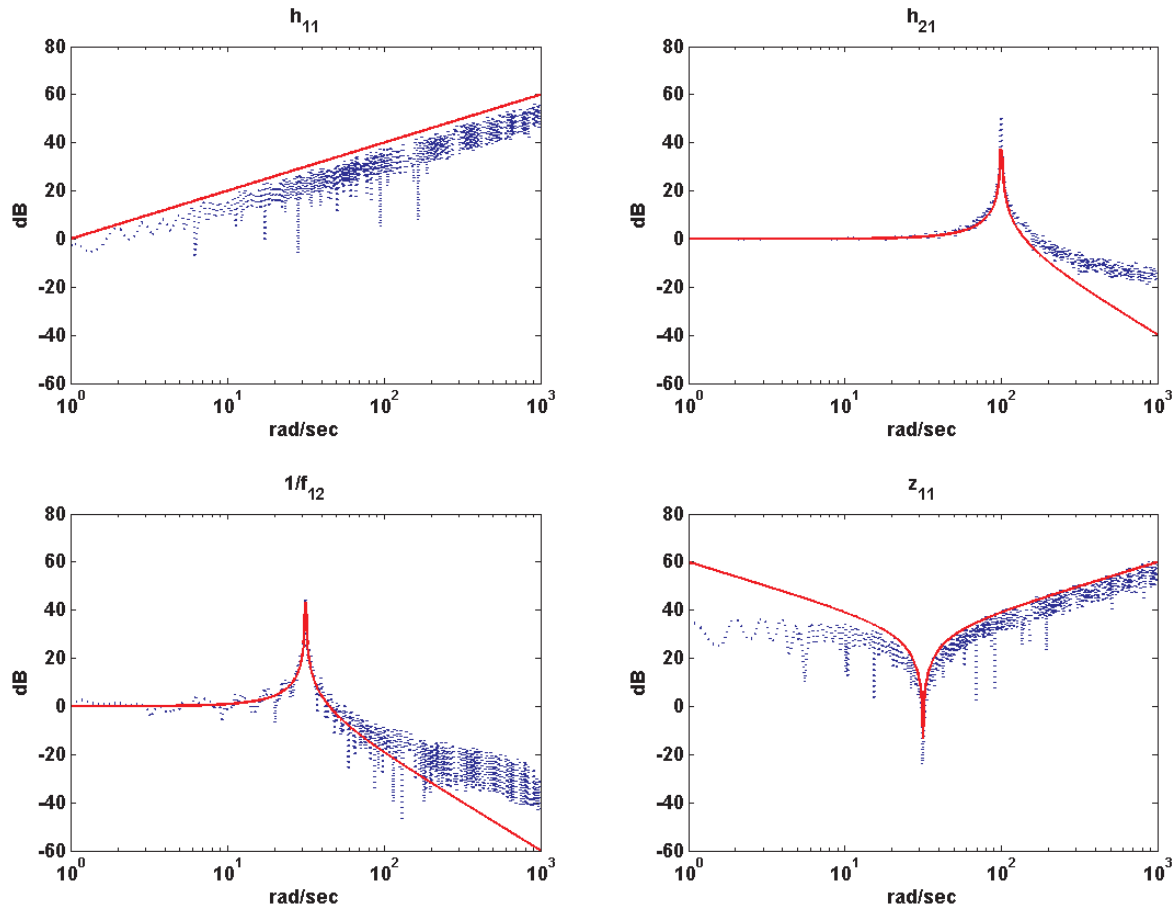


Fig. 9. Magnitudes of the performance indices for DFR teleoperation for large β with feedback of v_s and f_e when $R = 0.1$, $R' = 1$ and $\omega_0 = 100 \text{ rad s}^{-1}$. Simulation results (dashed) and idealized models (solid).

dissipates energy, which has a stabilizing effect (Diolaiti et al., 2006). Also, upper bounds on the dynamic ranges of the environment and operator impedances that exist in practice result in relaxed absolute stability conditions (Hashtrudi-Zaad and Salcudean, 2001). Even without taking friction or the limited dynamic range of environment and operator impedances into account, we have shown that teleoperation is absolutely stable with feedback of v_s alone, or v_e and v_s while Equation (35) is used for generating the desired trajectory of v_s .

Note that the absolute stability results in Table 1 are valid only for very large β : stability analysis for a limited β is complex and remains as future work.

7. Simulation Study

In order to confirm the transparency results of Table 1, we simulated the PEB and DFR teleoperation control architectures in MATLAB and SimuLink (The MathWorks, Inc., Natick, MA, USA) using a variable-step, continuous-time ode23 solver. We

chose $M_m = M_{sm} = 1 \text{ kg}$, $M_{se} = 0.1 \text{ kg}$, $k_s = 1000 \text{ N m}^{-1}$, and therefore $R = 0.1$, $R' = 1$ and $\omega_0 = 100 \text{ rad s}^{-1}$. Also, the control parameter $\beta = 10^6$ was chosen to be large as was assumed in Table 1. The excitation input f_h in Figure 5 consisted of the sum of a number of sinusoids evenly-spaced in the frequency domain from zero to $1,000 \text{ rad s}^{-1}$. The reason for this choice is that a multi-sine signal demonstrates a rich and almost uniform spectrum over the frequency range of interest and is a highly persistent excitation (*pe*) as the sum of n sinusoids is *pe* of an order not less than $2n - 2$ (Soderstrom and Stoica, 1989). Free-motion and hard-contact tests were simulated for 20 seconds using $k_e = 0$ and $k_e = 10^7 \text{ N m}^{-1}$, respectively. By applying spectral analysis (MATLAB function `spa`), h_{11} and h_{21} were estimated using the free-motion test data via Equation (5), and $1/f_{12}$ and z_{11} were estimated using the hard-contact test data via Equation (7). As an example, the estimated magnitudes of the performance indices for DFR teleoperation with feedback of v_s and f_e are shown in Figure 9 (dashed lines), which closely follow the idealized indices listed in the fourth column of Table 1 (solid lines).

8. Discussion and Concluding Remarks

The results of the above analysis as listed in Table 1 are mainly useful for understanding how extra sensors at the tip of a flexible slave robot can enhance transparency. With minimally invasive surgical robots as one of the candidates for which such an analysis is justified, however, arguments against adding sensors at the robot tip are made based on the fact that such sensors can complicate the design of the robotic arm, create sterilization issues, and ultimately raise the cost of the system. As a result, tip sensors have so far been avoided in today's commercial surgical systems (e.g. the da Vinci system from Intuitive Surgical Inc., Sunnyvale, CA, USA). On the other hand, in the specific example of the da Vinci robot, in order to avoid joint compliance, tensions in the cable drives are high. This has resulted in large friction in the instruments' drive trains, requiring sizable, remotely-based motors for tip actuation. In general, however, given the trade-off between joint compliance and friction in cable drives, joint compliance should be addressed separately especially in robots that are designed to be lightweight and cannot accommodate large actuators. Therefore, the questions addressed in this paper were, regardless of the state of sensor/actuator technologies in terms of meeting the requirements for integration in surgical or space robots, what are the limitations imposed by the slave robot flexibility on teleoperation transparency, what added benefits can tip sensors deliver during teleoperation with a flexible slave, and what are the cost-benefit tradeoffs of reducing or eliminating the effect of flexibility in haptic teleoperation?

- When the slave is in free space, unlike DFR teleoperation in which the user only feels the master inertia, in PEB teleoperation the user feels an additional impedance (which can be large – note the highly viscous term s^3 in the third column of Table 1). Such a residual impedance can create problems in terms of detecting small contacts or contact with very soft tissue, and a force sensor at the slave helps to avoid it.
- For both PEB and DFR teleoperation architectures, velocity (or position) feedback from the tip of the flexible slave improves free-space position tracking performance at higher frequencies, which is otherwise hampered by the anti-resonance of the two-mass-spring model unless Equation (35) is used for generating the desired slave velocity. It is of practical interest to maintain good position tracking bandwidth in order to enable accurate and fast manipulation.
- In DFR teleoperation, tip velocity feedback or using Equation (35) for calculating the desired slave velocity improves hard-contact force tracking performance. Otherwise, force tracking response will be band-limited, and the system will not be able to accurately simulate high-frequency haptic phenomena such as edges or surface

texture of an object. Also, low-bandwidth haptic feedback has previously been shown to increase subjective workload in hard-contact assembly tasks.

- Over low frequencies, free-space position tracking and hard-contact force tracking are both satisfactory even in the absence of tip velocity feedback. However, in terms of the transmitted impedance, we showed that the only way to eliminate the display of robot flexibility to the user (even over low frequencies) is to either use tip velocity feedback or use Equation (35) for generating the desired slave velocity. Previously, Christiansson and van der Helm (2007) had concluded through experimental measurements with a low-stiffness slave that the maximum transmitted impedance can be doubled if tip velocity feedback is used in a four-channel bilateral teleoperation architecture. Consistent with their results, we show that tip velocity feedback helps achieve an infinitely stiff transmitted impedance ($z_{11} \rightarrow \infty$) in theory even with PEB and DFR teleoperation architectures, which have lower implementation complexity. The significance of this result is in the fact that if the robot flexibility is transmitted to the user, it will limit the perception of hitting a hard object (such as bone) and will make it more difficult to utilize haptic cues for soft-tissue stiffness discrimination. This has direct consequences, for example, in tissue palpation as a means to detect cancerous tissue, which has a different stiffness compared to healthy tissue.

Clearly, implementation issues are also important. While performance and stability benefit when Equation (35) is used for generating the desired slave velocity, the trade-off is that obtaining low-noise velocity and force information for differentiation in Equation (35) is problematic. Nevertheless, instead of using sensors to measure the end-effector velocity v_e and the external force f_e , these quantities may be estimated using an extended state observer (Zhang and Tong, 2006) for less noisy signals. Evaluating the usefulness of such an observer remains as future work.

Looking beyond flexibility, backlash in the joints of a slave robot also has adverse effects on the transparency and stability of teleoperation. Surgical robots are a typical example of teleoperation systems with backlash due to the presence of cable-driven end-effectors. A similar analysis on the effect of backlash during bilateral teleoperation may quantify the problem and reveal ways to minimize it.

Acknowledgments

This research was supported by the National Science Foundation grant EEC-9731748 and a postdoctoral fellowship

awarded to the first author by the Natural Sciences and Engineering Research Council of Canada. The authors acknowledge the helpful discussions with Allison M. Okamura (Johns Hopkins Laboratory for Haptic Exploration) and Katherine J. Kuchenbecker (University of Pennsylvania GRASP Lab).

References

- Abbott, J. and Okamura, A. (2005). Effects of position quantization and sampling rate on virtual wall passivity. *IEEE Transactions on Robotics*, **21**(5): 952–964.
- Aliaga, I., Rubio, A. and Sanchez, E. (2004). Experimental quantitative comparison of different control architectures for master–slave teleoperation. *IEEE Transactions on Control Systems Technology*, **12**(1): 2–11.
- Aziminejad, A. et al. (2007). Wave-based time delay compensation in bilateral teleoperation: two-channel versus four-channel architectures. *Proceedings of the American Control Conference*, New York, pp. 1449–1454.
- Beasley, R. A. and Howe, R. D. (2005). Model-based error correction for flexible robotic surgical instruments. *Proceedings of Robotics: Science and Systems Conference*, Cambridge, MA, pp. 359–364.
- Cannon, R. H. and Schmitz, E. (1984). Initial experiments on the end-point control of a flexible one-link robot. *The International Journal of Robotics Research*, **3**(3): 62–75.
- Ching, H. and Book, W. (2006). Internet-based bilateral teleoperation based on wave variable with adaptive predictor and direct drift control. *Journal of Dynamic Systems, Measurement, and Control*, **128**(1): 86–93.
- Chopra, N. et al. (2006). On tracking performance in bilateral teleoperation. *IEEE Transactions on Robotics*, **22**(4): 861–866.
- Christiansson, G. A. V. and van der Helm, F. C. T. (2007). The low-stiffness teleoperator slave—a trade-off between stability and performance. *The International Journal of Robotics Research*, **26**(3): 287–299.
- Colgate, J. E. and Brown, J. M. (1994). Factors affecting the Z-width of a haptic display. *Proceedings of the IEEE International Conference on Robotics and Automation*, Los Alamitos, CA, pp. 3205–3210.
- Diaz, I. and Gil, J. J. (2008). Influence of internal vibration modes on the stability of haptic rendering. *Proceedings of the IEEE International Conference on Robotics and Automation*, Pasadena, CA.
- Diolaiti, N. et al. (2006). Stability of haptic rendering: Discretization, quantization, time delay, and Coulomb effects. *IEEE Transactions on Robotics*, **22**(2): 256–268.
- Dwivedy, S. K. and Eberhard, P. (2006). Dynamic analysis of flexible manipulators, a literature review. *Mechanism and Machine Theory*, **41**(7): 749–777.
- Gil, J. et al. (2004). Stability analysis of a 1 dof haptic interface using the Routh–Hurwitz criterion. *IEEE Transactions on Control Systems Technology*, **12**(4): 583–588.
- Hannaford, B. (1989). A design framework for teleoperators with kinesthetic feedback. *IEEE Transactions on Robotics and Automation*, **5**: 426–434.
- Hashtrudi-Zaad, K. and Salcudean, S. E. (2001). Analysis of control architectures for teleoperation systems with impedance/admittance master and slave manipulators. *The International Journal of Robotics Research*, **20**(6): 419–445.
- Haykin, S. (1970). *Active Network Theory*. Reading, MA, Addison-Wesley.
- Love, L. and Book, W. (1995). Contact stability analysis of virtual walls. *Proceedings of the ASME International Mechanical Engineering Conference and Exposition*, **57**: 689–694.
- Mills, J. K. (1992). Stability and control of elastic-joint robotic manipulators during constrained-motion tasks. *IEEE Transactions on Robotics*, **8**(1): 119–126.
- Niemeyer, G. and Slotine, J. J. E. (2004). Telemanipulation with time delays. *The International Journal of Robotics Research*, **23**(9): 873–890.
- Nishida, S. and Yoshikawa, T. (2003). Space debris capture by a joint compliance controlled robot. *Proceedings of IEEE/ASME International Conference on Advanced Intelligent Mechatronics*, Vol. 1, Kobe, Japan, pp. 496–502.
- Ohnishi, H. and Mochizuki, K. (2007). Effect of delay of feedback force on perception of elastic force: a psychophysical approach. *IEICE Transactions on Communications*, **E90-B**(1): 12–20.
- Pressman, A. et al. (2007). Perception of delayed stiffness. *The International Journal of Robotics Research*, **26**(11–12): 1191–1203.
- Soderstrom, T. and Stoica, P. (1989). *System Identification*. Englewood Cliffs, NJ, Prentice-Hall.
- Spong, M. W. (1987). Modeling and control of elastic joint robots. *ASME Journal of Dynamic Systems, Measurement and Control*, **109**(4): 310–319.
- Tavakoli, M. et al. (2007a). High-fidelity bilateral teleoperation systems and the effect of multimodal haptics. *IEEE Transactions on Systems, Man and Cybernetics—Part B*, **37**(6): 1512–1528.
- Tavakoli, M. et al. (2007b). Stability of discrete-time bilateral teleoperation control. *Proceedings of 2007 International Conference on Intelligent Robots and Systems*, San Diego, CA, pp. 1624–1630.
- Tavakoli, M. and Howe, R. D. (2007). The effect of joint elasticity on bilateral teleoperation. *Proceedings of the 2007 IEEE/RSJ International Conference on Intelligent Robots and Systems*, San Diego, CA, pp. 1618–1623.
- Tavakoli, M. and Howe, R. D. (2008). Haptic implications of tool flexibility in surgical teleoperation. *Proceedings of the 16th Symposium on Haptic Interfaces for Virtual Environ-*

- ments and Teleoperator Systems*, Reno, NV, March 2008, pp. 377–378.
- Vukosavic, S. N. and Stojic, M. R. (1998). Suppression of torsional oscillations in a high-performance speedservo drive. *IEEE Transactions on Industrial Electronics*, **45**(1): 108–117.
- Zhang, G. and Furusho, J. (2000). Speed control of two-inertia system by PI/PID control. *IEEE Transactions on Industrial Electronics*, **47**(3): 603–609.
- Zhang, R. and Tong, C. (2006). Torsional vibration control of the main drive system of a rolling mill based on an extended state observer and linear quadratic control. *Journal of Vibration and Control*, **12**(3): 313–327.
- Zhu, G., Ge, S. S. and Lee, T. H. (1999). Simulation studies of tip tracking control of a single-link flexible robot based on a lumped model. *Robotica*, **17**(1): 71–78.